Journal of Alloys and Compounds, 185 (1992) 207–219
JALCOM 249

Electromigration and residual resistivity of hydrogen in row 5 and 6 transition metals

J. van Ek and A. Lodder
Faculteit der Natuurkunde en Sterrenkunde, Vrije Universiteit, De Boelelaan 1081, 1081 HV Amsterdam (Netherlands)

(Received November 25, 1991)

Abstract

Both the electromigration wind valence and the residual resistivity for hydrogen in all row 5 (yttrium to silver) and row 6 (lanthanum to gold) transition metals were calculated. Host metals with a hexagonal lattice have been treated in the f.c.c. or b.c.c. structure. The Korringa–Kohn–Rostoker–Green function method, used to describe the multiple scattering of Bloch electrons, accounts for charge transfer and lattice deformation around the interstitial hydrogen.

1. Introduction

Diffusive motion of interstitial and substitutional impurities in metals, being random in itself, can be directed by applying an electric field **E** to the sample. The susceptibility of the impurity to **E** is given by the effective valence Z^* of the impurity in a certain metal. Thus the phenomenological expression for the driving force **F** in electromigration reads as

$$\mathbf{F} = Z^* e \mathbf{E} \tag{1}$$

The elementary charge $e \equiv |e|$ equals $2^{1/2}$ in Rydberg atomic units used throughout ($\hbar = 1$, $m_e = \frac{1}{2}$), unless otherwise indicated. In the theory of electromigration a distinction is usually made between two contributions to the driving force, as follows.

The direct force $\mathbf{F}_{\text{direct}} = Z_{\text{direct}} e\mathbf{E}$ measures the electrostatic force on the impurity in the electron gas. Although the direct force constitutes a conceptually simple quantity, the question whether or not impurity screening is complete (*i.e.* $\mathbf{F}_{\text{direct}} \equiv 0$) is at the basis of fierce debate in electromigration literature [1–9].

In dilute metal–impurity systems Bloch electrons in the current are scattered by impurity-induced defect clusters in the lattice. This impurity scattering gives rise to finite mean-free-path lengths for the electrons in Bloch states. At low enough temperatures the electric current is given by the field divided by the residual resistivity ρ_0. In the simple ballistic picture the current-carrying electrons form the so-called electron wind. The ballistic model [1, 2] assumes that a free electron gas at density n does gain a

momentum of $-n\tau e\mathbf{E}$ per unit volume. The transport relaxation time τ is characteristic for the electron gas under consideration. During collisions of the electrons with impurities, at density n_i, this momentum gain is transferred to the impurities at a frequency equal to the inverse impurity relaxation time τ_i^{-1}. The average force on the impurities thus reads $\mathbf{F}_{\text{wind}} = -(n\tau/n_i\tau_i)e\mathbf{E} = -(n\rho_0/n_i\rho)e\mathbf{E}$, since for free electrons $\rho \propto \tau^{-1}$ and $\rho_0 \propto \tau_i^{-1}$, and will point in a direction opposite to that of the external field. This is the wind force.

Summarizing, the driving force in eqn. (1) can be written as the sum of a direct and a wind part

$$\mathbf{F} = \mathbf{F}_{\text{direct}} + \mathbf{F}_{\text{wind}} = (Z_{\text{direct}} + Z_{\text{wind}})e\mathbf{E} \tag{2}$$

Only the sum $Z^* = Z_{\text{direct}} + Z_{\text{wind}}$ can be obtained from experiment (for an overview see ref. 10).

The direct force is not very accessible through a computational study. The treatment of self-consistent screening of an impurity cluster is a complicated problem involving interacting electrons in scattering states at all energies. Above all it is not clear how the direct force should be extracted from the self-consistent scattering states. On the other hand, scattering quantities for Bloch electrons at the Fermi energy ϵ_F in principle can be calculated within a multiple-scattering formulation, given a potential. Among these are the wind valence Z_{wind} and the residual resistivity ρ_0.

The research field of hydrogen in metals has known a period of great interest [11]. Now that experimental activity in the field has declined, some unclarified but intriguing observations are still calling for an explanation. For instance the observed differences in sign of Z_{wind} in the group 5b transition metals vanadium, niobium and tantalum as well as the small but significant H–D isotope effect in Z^* in these metals [12] but also in nickel [13] and palladium [14] can be mentioned. In turn it is surprising that the residual resistivity in the hydrides of these metals does not show a measurable isotope effect [15–17].

This paper is devoted to dilute metal–hydrogen systems. From a computational point of view these systems form an attractive subject. First of all, the multiple-scattering problem for an impurity cluster embedded in an otherwise perfect metallic host can be solved (see for instance refs. 18 and 19). In this Korringa–Kohn–Rostoker(KKR)–Green function approach the band structure as well as charge transfer and lattice deformation are accounted for. Further, the lack of self-consistent impurity potentials for interstitial hydrogen might well be counterbalanced by the relative simplicity of the electronic structure of the hydrogen atom.

In Section 2 the method used in calculating Z_{wind} and ρ_0 from the alloy wave function will be outlined briefly. In section 3 results of calculations of these two quantities for hydrogen in all fifth- and sixth-row transition metals will be presented. A discussion of some general trends is given in Section 4. Also attention is paid to cases where experimental data exist. Section 5 summarizes the main points made in this paper.

2. Outline of the method

The deviation from the equilibrium distribution function for the electrons, linear in the externally applied field, reads as

$$g_{n\mathbf{k}} = -e\boldsymbol{\Lambda}_{n\mathbf{k}} \cdot \mathbf{E}\left(-\frac{\partial f^0(\epsilon_{n\mathbf{k}})}{\partial \epsilon}\right) \tag{3}$$

The vector mean free path $\boldsymbol{\Lambda}_{n\mathbf{k}}$ applies to electrons in states labelled $n\mathbf{k}$ at energy $\epsilon_{n\mathbf{k}}$. Since at moderate temperatures the negative energy derivative of the Fermi–Dirac distribution function $f^0(\epsilon)$ can be approximated by a delta function at ϵ_F, summations over all states weighted by $g_{n\mathbf{k}}$ reduce to Fermi surface integrals. This greatly facilitates the calculation of transport properties that are related to the electron current.

In order to calculate the matrix elements occurring in the expression for the wind force [20]

$$\mathbf{F}_{\text{wind}}(\mathbf{R}_1) = \sum_{n\mathbf{k}} g_{n\mathbf{k}} \langle \bar{\Psi}_{n\mathbf{k}}(\mathbf{r};\, \mathbf{R}_1) | -\nabla_{\mathbf{R}_1} v_1(\mathbf{r}-\mathbf{R}_1) | \bar{\Psi}_{n\mathbf{k}}(\mathbf{r}:\, \mathbf{R}_1) \rangle$$

$$= \underline{Z}_{\text{wind}}(\mathbf{R}_{1)e}\mathbf{E} \tag{4}$$

solutions $\bar{\Psi}_{n\mathbf{k}}$ to the Schrödinger equation for the perturbed crystal

$$(H^{\text{crystal}} - \epsilon_{n\mathbf{k}} + \Delta V)\bar{\Psi}_{n\mathbf{k}} = 0 \tag{5}$$

are needed at $\epsilon_{n\mathbf{k}} = \epsilon_F$. The potential v_1 of the migrating atom in the force operator $-\nabla_{\mathbf{R}_1} v_1(\mathbf{r}-\mathbf{R}_1)$ in eqn. (4) is also contained in the total perturbing potential ΔV. The crystal hamiltonian $H^{\text{crystal}} = p^2 + V^{\text{crystal}}$ is the usual single-particle hamiltonian for the perfect crystal in the local density approximation.

The solution to eqn. (5) is obtained in terms of the crystal or host Green function G^{crystal} and the Bloch wave functions $\Psi_{n\mathbf{k}}$ as the unperturbed reference-system wave functions. The formal operator expressions read as

$$\bar{\Psi}_{n\mathbf{k}} = \Psi_{n\mathbf{k}} + G^{\text{crystal}}\, \Delta V \bar{\Psi}_{n\mathbf{k}} \tag{6}$$

with

$$(p^2 + V^{\text{crystal}} - \epsilon_F) G^{\text{crystal}} = 1 \tag{7}$$

and

$$(p^2 + V^{\text{crystal}} - \epsilon_F)\Psi_{n\mathbf{k}} = 0 \tag{8}$$

When both V^{crystal} and ΔV are muffin tin (MT) potentials eqn. (8) gives the famous KKR equations [21, 22] while eqn. (6) can be developed [18] to yield

$$\bar{\Psi}_{n\mathbf{k}}(\mathbf{x}+\mathbf{R}_p) = \sum_{Lj'L'} R_{pL}(\mathbf{x}) A_{pLj'L'} C_{j'L'}(n\mathbf{k}) \tag{9}$$

with host wave function coefficients $C_{jL}(n\mathbf{k})$ at lattice site j, $L \equiv (l,\, m)$, backscattering matrix A and regular solutions $R_{pL}(\mathbf{x})$ pertaining to the MT potential centred around $\mathbf{R}_p$. The A matrix contains all multiple-scattering

effects induced by the perturbing potential. Detailed information on how this complex quantity (in both senses) is actually calculated can be found elsewhere [18, 23, 24].

For MT potentials the integration over direct space in eqn. (4) can be evaluated analytically [20]. After replacement of the summation over states labelled $n\mathbf{k}$ by a Brillouin zone integral, vectorial Fermi surface integrals that remain are of the type

$$\mathbf{I}_{pLp'L'} = \frac{1}{V_{\mathrm{BZ}}} \int_{\mathrm{FS}} \frac{\mathrm{d}S_{n\mathbf{k}}}{V_{n\mathbf{k}}} C^*_{pL}(n\mathbf{k}) \boldsymbol{\Lambda}_{n\mathbf{k}} C_{p'L'}(n\mathbf{k}) \tag{10}$$

and can be calculated efficiently using point group symmetry [25].

Interestingly integrals of the same type as eqn. (10) occur in the evaluation of the residual resistivity from the vector mean free path $\boldsymbol{\Lambda}^{\mathrm{imp}}_{n\mathbf{k}}$ in electron impurity scattering:

$$\rho_0{}^{-1} = \frac{4}{(2\pi)^3} \int_{\mathrm{FS}} \frac{\mathrm{d}S_{n\mathbf{k}}}{V_{n\mathbf{k}}} \mathbf{v}_{n\mathbf{k}} \times \boldsymbol{\Lambda}^{\mathrm{imp}}_{n\mathbf{k}} \tag{11}$$

It is therefore not surprising that residual resistivity programs have been developed simultaneously with the wind force programs [26].

Although $\boldsymbol{\Lambda}^{\mathrm{imp}}_{n\mathbf{k}}$ and thus ρ_0 can be calculated truly *ab initio*, this is not the case for $\boldsymbol{\Lambda}_{n\mathbf{k}}$ in eqn. (3) to which all dissipative scattering mechanisms contribute. If the isotropic relaxation time approximation [27] is invoked, $\boldsymbol{\Lambda}_{n\mathbf{k}}$ equals $\tau \mathbf{v}_{n\mathbf{k}}$. The velocities are available (often strongly anisotropic over the Fermi surface) and τ is then calculated from the measured bulk conductivity at temperature T through

$$\rho(T)^{-1} = \frac{4\tau}{(2\pi)^3} \frac{1}{3} \int_{\mathrm{FS}} \mathrm{d}S_{n\mathbf{k}} v_{n\mathbf{k}} \tag{12}$$

The integral in eqn. (12) is evaluated over the Fermi surface of the pure host, obtained from a KKR calculation.

The potentials used in this work have been constructed from overlapping self-consistent relativistic atomic charge densities [28, 29]. The Slater exchange factor $\alpha = 1$ was used. The KKR programs underlying the calculation of $\bar{\Psi}_{n\mathbf{k}}$ for a given potential are non-relativistic. However, relativistic contraction effects in the orbital resolved charge densities are fully present in the atomic potentials, thus leading to relativistic contributions to the crystal potential, albeit in a non-self-consistent fashion. A previous study of the de Haas–van Alphen effect in Pd(H) [23] showed that potentials constructed in this way lead to a Fermi surface comparable with or even better than that resulting from the self-consistent potential of Moruzzi *et al.* [30]. For all the metals it has been verified that all parts of the Fermi surface that are not due to spin–orbit coupling are present with acceptable shapes (see for instance ref. 25 for niobium and palladium).

Charge neutrality in the system was imposed by requiring fulfilment of the generalized Friedel sum rule [31]. In practice [24] this was attained by

shifting the potentials of the first shell by a constant amount of energy until the total screening charge associated with the cluster potential was $Z=1$ for hydrogen.

Comparison of *ab initio* calculated residual resistivities with experimental data served in judging the quality of the potentials.

3. Results

Fifth-row transition metals (yttrium to silver) are characterized by a krypton noble gas core electron configuration and valence electrons in bands originating in 4d and 5s atomic orbitals. The first transition metal in row 6 is lanthanum with the $[Xe]5d^16s^2$ electronic configuration for the free atom. Lanthanum differs from the rest of the row 6 metals in that it does not have a filled 4f shell in addition to the xenon part of the core. The 4f shell is filled in the lanthanide series separating lanthanum from hafnium. It is known that f electrons are not very efficient in screening the nuclear charge [32, 33], resulting in a stronger attractive potential as seen by the electrons in the 5d6s valence shell. Relativistic contraction of mainly the valence s orbitals is an effect which points in the same direction. Along the columns of the periodic table this shows up in large changes of the lattice parameters when going from row 4 to row 5, but only small changes when going from row 5 to 6. Without exception the crystal structures for pairs of row 5–6 transition metals are the same, but the bonding energy per atom in row 6 is higher [34].

The structural similarity along the columns in the two rows offers the possibility of a direct comparison between Bloch electron scattering by hydrogen-induced defect clusters, as has been done earlier for Nb(H) *vs.* Ta(H) [24]. Being limited to f.c.c. and b.c.c. crystal structures all hexagonal lattices have been treated as in the f.c.c. structure. Only Zr(H) and Hf(H) have been studied in both the f.c.c. and b.c.c. structures. The lattice constants of the alternative structures are chosen in such a way that the atomic volume in the metal was left unchanged [30]. Whenever the difference in lattice parameter was less than 0.06 u the average value was taken for both metals. Table 1 shows the crystal structure, the lattice parameters and the Fermi energies as measured from the MT zero. The last column gives the valence electron configuration as used in the construction of the crystal potential. In order to retain enough of the scattering power of the interstitial the host MT radii are reduced from touching spheres to $0.325a$ for f.c.c. and $0.335a$ for b.c.c. metals. Here a is the lattice constant.

The equilibrium position for hydrogen in yttrium and lanthanum is the tetrahedral site in the true hexagonal structure. This was carried over to the f.c.c. structures, replacing the hexagonal lattice in the present calculation. The tetrahedral position in the f.c.c. lattice has T_d point group symmetry. The same assumption was made for the other hexagonal metals (zirconium, hafnium, technetium, rhenium, ruthenium, osmium). In the b.c.c. lattice the

TABLE 1

Lattice structures, lattice parameters a, Fermi energies ϵ_F and atomic configurations as used in computing Z_{wind} and ρ_0

Metal	Structure	a	ϵ_F	Atomic configuration
Y	f.c.c.	9.632	0.386	$4d^15s^2$
La	f.c.c.	10.031	0.350	$5d^16s^2$
Zr	b.c.c.	6.804	0.650	$4d^25s^2$
Hf	b.c.c.	6.734	0.740	$5d^26s^2$
Zr	f.c.c.	8.572	0.545	$4d^25s^2$
Hf	f.c.c.	8.484	0.634	$5d^26s^2$
Nb	b.c.c.	6.238	0.852	$4d^45s^1$
Ta	b.c.c.	6.238	0.927	$5d^36s^2$
Mo	b.c.c.	5.962	0.997	$4d^55s^1$
W	b.c.c.	5.962	1.129	$5d^46s^2$
Tc	f.c.c.	7.278	0.764	$4d^55s^2$
Re	f.c.c.	7.352	0.934	$5d^56s^2$
Ru	f.c.c.	7.214	0.780	$4d^75s^1$
Os	f.c.c.	7.214	0.963	$5d^66s^2$
Rh	f.c.c.	7.189	0.759	$4d^95s^0$
Ir	f.c.c.	7.254	0.948	$5d^86s^1$
Pd	f.c.c.	7.351	0.515	$4d^95s^1$
Pt	f.c.c.	7.408	0.778	$5d^96s^1$
Ag	f.c.c.	7.722	0.527	$4d^{10}5s^1$
Au	f.c.c.	7.722	0.713	$5d^{10}6s^1$

hydrogen atom occupies the tetragonally distorted tetrahedral position (point group D_{2d}). The octahedral position (O_h) is the equilibrium site for small interstitials in f.c.c. lattices. The interstitial MT radii are $0.108a$, $0.224a$ and $0.175a$ for the T_d, D_{2d} and O_h sites respectively.

In the present study only Z_{wind} and ρ_0 values at the equilibrium sites will be presented. Nevertheless it is perfectly possible to follow the impurity in its zero-point motion and to perform a quantum mechanical averaging with a probability density function. In this way even an experimentally observed H–D isotope effect in Z^* [12] and the lack of this effect in ρ_0 [17] could be explained [24, 26].

At octahedral and tetrahedral sites in the f.c.c. lattice $\underline{Z}_{wind}(\mathbf{R}_1)$ (see eqn. (4)) is an isotropic diagonal tensor. This does not hold for the b.c.c. equilibrium site. It was shown that, when the migration path of the proton is taken into account, only one component of the anisotropic diagonal tensor contributes [24]. The calculated scalar wind-valences are given in the third, fourth and fifth columns of Table 2. Residual resistivities obtained from the iterative solution of the Boltzmann equation (typically 4–10 iterations) are shown in columns 6–8. Both for Z_{wind} and ρ_0 each time the results for three impurity cluster configurations are given. First just the impurity in a perfect lattice, then the impurity plus charge transfer to the first shell and finally also a slight radial outward displacement of the first shell were accounted

TABLE 2

Wind valences Z_{wind} and residual resistivities ρ_0 ($\mu\Omega$ cm (at.%)$^{-1}$) for hydrogen in row 5 and row 6 transition metals

Metal	Structure	Z_{wind} [a]			ρ_0 [a]			τ [b]	$\frac{1}{3}\int_{FS} dS_{nk} v_{nk}$ [c]
		Impurity	+CT	+CT, LD	Impurity	+CT	+CT, LD		
Y	f.c.c.	−0.41	−0.41	−0.35	1.19	1.29	1.50	27	0.637
La	(tetrahedral)[d]	0.06	0.05	0.04	0.17	1.18	1.23	4	6.859
Zr	b.c.c.	−0.14	−0.13	−0.31	0.54	0.78	1.34	18	1.174
Hf	(tetrahedral)	−0.03	−0.04	−0.04	0.71	0.77	2.01	16	1.520
Zr	f.c.c.	−0.36	−0.36	−0.26	0.38	0.37	0.71	7	3.177
Hf	(tetrahedral)	0.46	0.46	0.41	0.24	0.28	0.65	2	10.66
Nb	b.c.c.	1.16	1.00	0.86	0.22	0.34	0.72	20	3.507
Ta	(tetrahedral)	−0.17	−0.17	−0.30	0.13	0.16	0.55	13	5.248
Mo	b.c.c.	−1.33	−3.50	−6.77	0.04	0.35	0.66	36	3.595
W	(tetrahedral)	−0.90	−1.21	−0.87	0.13	0.71	1.02	13	9.248
Tc	f.c.c.	−0.50	−0.47	−0.44	0.01	0.09	0.23	6	9.136
Re	(tetrahedral)	0.02	0.02	0.01	0.01	0.09	0.22	7	6.643
Ru	f.c.c.	−0.41	−0.31	−0.10	0.01	0.11	0.23	14	7.353
Os	(tetrahedral)	0.00	0.00	0.00	0.00	0.06	0.19	4	6.396
Rh	f.c.c.	−0.08	0.01	−0.03	0.00	0.06	0.22	29	5.525
Ir	(octahedral)	0.00	0.00	0.00	0.00	0.06	0.23	4	5.430
Pd	f.c.c.	−0.70	−0.70	−0.77	0.00	0.30	0.52	64	1.427
Pt	(octahedral)	0.03	0.01	0.02	0.00	0.07	0.23	5	16.32
Ag	f.c.c.	−33	−33	−35	2.11	2.11	2.19	201	2.406
Au	(octahedral)	−5.6	−6.5	−6.9	0.21	0.41	0.46	86	4.048

[a]Results are given for the impurity only, including charge transfer (+CT) and including charge transfer and lattice deformation (+CT, LD).
[b]Transport relaxation time.
[c]The velocity integral as it occurs in eqn. (12) in the text.
[d]Impurity site.

for. In the present calculations values of $0.01a$ around the octahedral position in an f.c.c. metal and $0.02a$ around the tetrahedral position in f.c.c. and b.c.c. lattices were used. This choice for the displacements was prompted by the self-consistent effective-medium calculations of Puska and Nieminen [35]. The site occupied by the proton is indicated in the second column of Table 2. There is no need to account for a second shell of surrounding atoms [36–38].

In most cases the atomic ground state configuration as given in the periodic table of the elements was used in constructing the crystal potentials. Exceptions are made for the Pd–Pt and Rh–Ir couples (see Table 1).

The d^9s^1 configuration for palladium has already been shown to give a good description of the palladium Fermi surface and de Haas–van Alphen scattering quantities (Dingle temperatures and cross-sectional area changes) in Pd(H) [23]. For this reason it seemed worthwhile to consider both the d^9s^1 and the $d^{10}s^0$ ground state configuration for the Pt atoms in the host crystal. In Pt(H) the differences in Z_{wind} and ρ_0 for these two configurations turned out to be very small. With Pt($d^{10}s^0$) the values $Z_{\text{wind}} = 0.03$ and $\rho_0 = 0.24$ $\mu\Omega$ cm (at.%)$^{-1}$ were obtained. These calculations account for the effect of charge transfer and lattice relaxation and should therefore be compared with the corresponding values in the fifth and eighth columns of Table 2.

For the residual resistivity in the hydrides of Rh(d^8s^1) and Ir(d^7s^2) no alarming deviations from the corresponding values in Table 2 were found ($\rho_0 = 0.28$ and 0.32 $\mu\Omega$ cm (at.%)$^{-1}$ respectively). However, the wind valence in these metals turned out to be sensitive to the configuration used. For Rh(H) and Ir(H) wind valences $Z_{\text{wind}} = -1.55$ and $+3.44$ respectively have been calculated. Although on a computational basis alone the large positive value in Ir(H) cannot be excluded, it certainly would represent an enigmatic exception among the generally negative or moderately positive wind valences in Fig. 1. Therefore it was preferred to use the results based on the Rh(d^9s^0) and Ir(d^8s^1) hosts as the representative values.

The last two columns of Table 2 show the values of the transport relaxation time τ, as calculated from the bulk resistivity at 900 K by means of eqn. (12), and the velocity integral $\frac{1}{3}\int_{\text{FS}} \mathrm{d}S_{n\mathbf{k}} v_{n\mathbf{k}}$. This relatively high temperature was chosen since, in order to enhance the mobility of the interstitials, most electromigration experiments will be done in this temperature region. Of course wind valences at lower temperatures can also be obtained by inserting the appropriate value of $\rho(T)$ into eqn. (12). Due to an increase of τ the magnitude of Z_{wind} will increase. (See for example Nb(H) and Ta(H) in ref. 24, where $T = 375$ K.)

4. Discussion

The numerical data on Z_{wind} and ρ_0 in Table 2 are represented graphically in Fig. 1 and Fig. 2 respectively. To guide the eye the values from complete calculations in a row (columns 5 and 8 of Table 2) have been connected

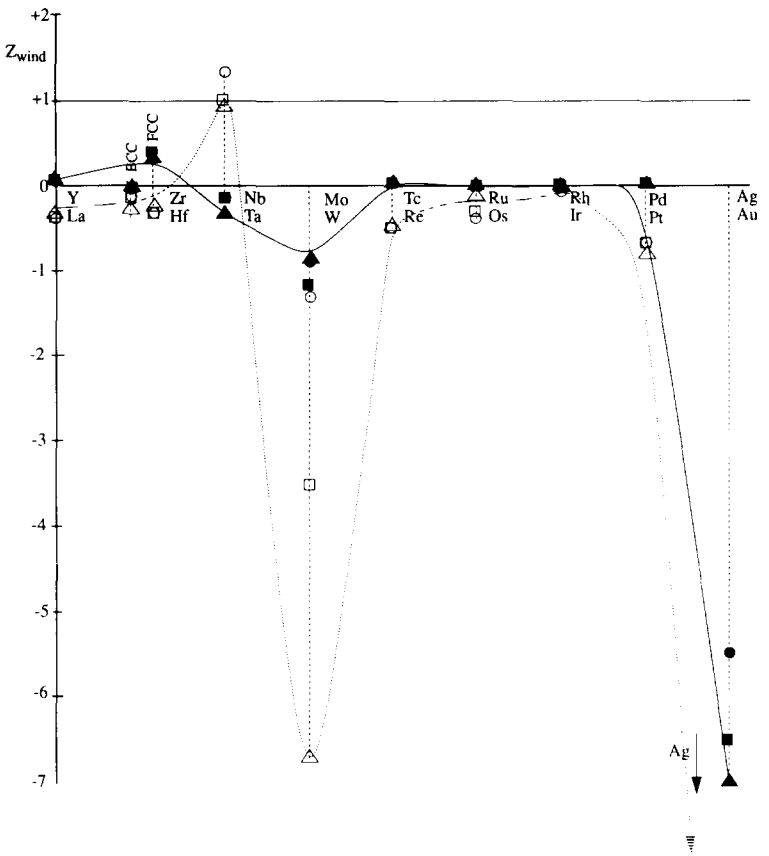

Fig. 1. Wind valence for hydrogen in row 5 (○, □, △) and row 6 (●, ■, ▲) transition metals: ○, ●, calculations for just the impurity; □, ■, calculations for an impurity plus charge transfer; △, ▲, complete calculations, also accounting for lattice deformation.

by a line. Since zirconium and hafnium are in their hexagonal phase at $T = 900$ K, the f.c.c. results are implicated in the interpolation. The horizontal line at $Z_{wind} = +1$ in Fig. 1 serves as an indication of the direct valence part of Z^*. In a previous study it was found that Z_{direct} was always reasonably close to unity ($0.7 < Z_{direct} < 1.5$). This could be deduced from measured Z^* values and calculated Z_{wind} values for hydrogen in nickel, palladium, vanadium, niobium and tantalum [24].

Because of structural differences between the host lattices and owing to different equilibrium sites for hydrogen in the various metals, no clear trends in Z_{wind} and ρ_0 are to be expected along the fifth or sixth row. Interesting comparisons in the columns can be made.

From Fig. 1 and Table 2 it should be noted that the presence of a first shell, possibly deformed, does influence Z_{wind} to a varying extent. Except in Mo(H) the effect of lattice distortion is moderate, indicating that the wind

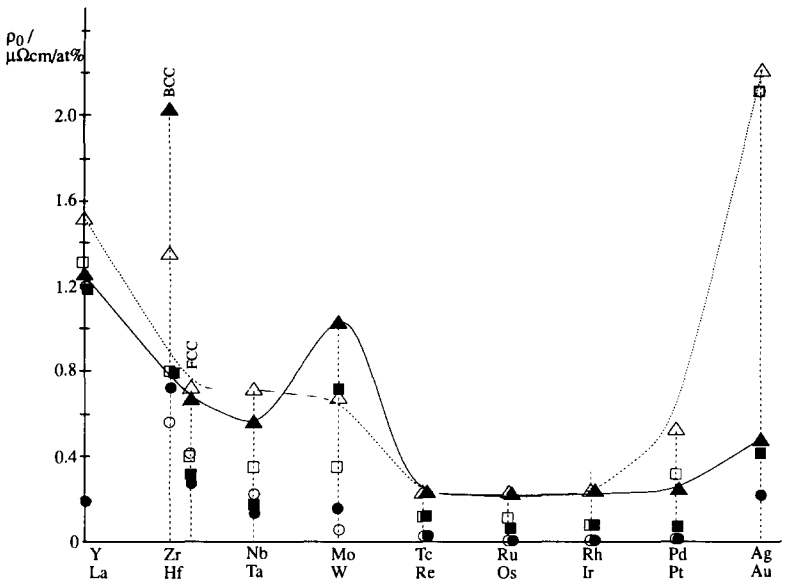

Fig. 2. Residual resistivity for hydrogen in row 5 (○, □, △) and row 6 (●, ■, ▲) transition metals (symbols as in Fig. 1).

valence mostly is a property of the interstitial itself immersed in an electron gas with certain characteristics depending on the host metal.

For the residual resistivity (Fig. 2) the situation is different. Generally a strong dependence of ρ_0 on the presence of the first shell emerges. Conspicuous are hydrogen in technetium, rhenium, ruthenium, osmium, rhodium, iridium, palladium and platinum. Just a proton in the otherwise perfect lattice gives a vanishingly small resistivity increase. Only inclusion of the first shell leads to values of ρ_0 that, for instance for Pd(H), compare well with experiment [26]. Such behaviour might be understood in view of the anti-bonding part of the d band that is getting filled. At ϵ_F the atomic d orbitals are combined in an anti-bonding fashion which results in a low density of conduction electrons at the octahedral and tetrahedral sites. This means that the density of conduction electrons taking part in impurity scattering at the interstitial sites will be low when compared with the early fifth- and sixth-row transition metals. The residual resistivity in yttrium, lanthanum, zirconium, hafnium, niobium and tantalum due to only the proton reflects this.

The influence of a radially outward displacement of the first shell atoms on ρ_0 should be interpreted in terms of the character of the conduction electrons at ϵ_F. When truly delocalized s electrons take care of the conduction, as in silver and gold, great sensitivity to the precise position of the first-shell atoms is not expected. More localized d electrons at ϵ_F were found to be rather sensitive to lattice deformation from calculations of the resistivity

increase due to lattice deformation in pure niobium and palladium [26]. Such behaviour is clearly reflected in the table: from Zr(H) or Hf(H) up to Pd(H) or Pt(H) displacement of the first shell results in a 50–150% increase in ρ_0. Y(H) and La(H) can be considered as intermediate cases since the d band starts getting filled in these metals. For Ag(H) or Au(H) this influence of local lattice deformation is found to be small.

On the whole the wind valences for the fifth row are more negative than those for the sixth row. A clear exception is formed by the Nb–Ta couple. Similarly the ρ_0 values for the fifth row are larger than those for the sixth row. Here the b.c.c. metal couples Mo–W and Zr–Hf form an exception. Although the simple ballistic model cannot be expected to be valid in detail, these general observations are in line with it. Differences in Z_{wind} and ρ_0 between row 5 and row 6 metals in the same group are easily understood for the Ag–Au pair. A much larger ρ_0 value in Ag(H) than in Au(H) also implies, according to the old ballistic model, a much larger negative wind valence in Ag(H). The lower resistivity in Au(H) is due to the higher velocity of the s-like Bloch electrons which, at the same electron density, can carry higher current densities. In none of the other metals is the situation as simple. It was shown previously [24] that the value of Z_{wind} is determined by the field-induced charge distribution around the proton only, while ρ_0 is determined by the whole impurity cluster. This model explains the difference in sign as observed in the experimentally well-known systems Nb(H) and Ta(H). A positive wind valence corresponds to an electric dipole around the proton directed opposite to the external field. The dipolar charge distribution exerts a wind force on the attractive hydrogen potential in the direction of **E**, so $Z_{\text{wind}} > 0$ in Nb(H). For Ta(H) the situation turned out to be more or less reversed, giving $Z_{\text{wind}} < 0$ in agreement with experiment too. Note from Fig. 1 that the positive wind valence for Nb(H) almost forms an exception among the dilute transition metal hydrides.

Also in agreement with experiment is the sign of Z_{wind} in Y(H) [39], although its calculated magnitude is too small. This in turn is consistent with an *ab initio* calculated ρ_0 which is too small as well (experimentally $\rho_0 = 3.10\ \mu\Omega\ (\text{at.}\%)^{-1}$ [40]). Probably the difference between hexagonal yttrium and f.c.c. yttrium will have contributed to this discrepancy. The results for Pd(H) are found to be in agreement with experiment. Calculated wind valences in Ag(H) are more negative than measured, according to the ballistic model compatible with an overestimated ρ_0 value.

It is possible to give a rough estimate of the influence on Z_{wind} of the substitution of the f.c.c. lattice for the hexagonal lattice. On the basis of the simple ballistic model, mentioned in the introductory paragraph, an anisotropic bulk resistivity directly influences the wind valence. For some hexagonal metals the anisotropy in $\rho(T)$ is known over a wide temperature range [41]. The ratio of $\rho_{\parallel}(900\ \text{K})$ (*i.e.* resistivity parallel to the basal plane) and $\rho_{\perp}$ (900 K) (perpendicular to the basal plane) equals 1.3, 1.5 and 1.5 for yttrium, rubidium and osmium respectively. A directional preference in the hydrogen motion (diffusion) could then result in

differences ranging from ± 15 to $\pm 25\%$ with respect to a simple average of $\rho_{\parallel}$ and $\rho_{\perp}$.

In view of the lack of consensus concerning the magnitude of the direct valence it is worthwhile to draw attention to the systems for which the wind valence is very small, namely the hydrides of rhenium, osmium, rhodium, iridium and platinum. Such systems in principle provide a unique opportunity to investigate the direct valence almost directly.

5. Conclusions

Wind valences and residual resistivities for hydrogen in all transition metals in the fifth and sixth rows of the periodic table have been calculated. Metals with a hexagonal lattice have been treated as f.c.c. or b.c.c. systems. For hexagonal and b.c.c. metals the tetrahedral position was chosen as the equilibrium position for the proton, in f.c.c. metals it was the octahedral site.

The vanishingly small ρ_0 values of just a proton in an otherwise perfect lattice of technetium, rhenium, rubidium, osmium, rhodium, iridium, palladium and platinum can be understood in terms of the anti-bonding character of the states at the Fermi level. Accounting for a first shell of metal atoms resulted in appreciable values for ρ_0.

In most cases the wind valence was found to be much less sensitive to the presence of a perturbed first shell than ρ_0. This clearly illustrates the fact that the wind valence comes about through the electron density directly around the proton. The wave function at the interstitial obviously is not very sensitive to alterations in the first shell, except for Mo(H). From the residual resistivity calculations it is concluded that the alloy wave function as a whole is influenced greatly by the first shell.

The calculated values for Z_{wind} and ρ_0 presented in this paper can serve as a guideline for future experiments. Estimates of Z_{wind} at temperatures T other than 900 K can easily be obtained by multiplying with a factor $\rho(900)/\rho(T)$. Direct measurement of Z_{direct} might be possible in those systems where Z_{wind} turned out to be very small.

Altogether it must be concluded that multiple-scattering theory, developed in the KKR–Green function formalism, provides an excellent tool. Both electromigration of hydrogen in transition metals and the residual resistivity caused by the hydrogen have become much more transparent. Predictions were made. Experimental confirmation is awaited.

Acknowledgment

One of the authors (J. van Ek) wishes to refer to the discussion with Dr. B. Drittler that induced the present work.

References

1 V. B. Fiks, *Sov. Phys. — Solid State, 1* (1959) 14.
2 H. B. Huntington and A. R. Grone, *J. Phys. Chem. Solids, 20* (1961) 76.
3 C. Bosvieux and J. Friedel, *J. Phys. Chem. Solids, 23* (1962) 123.
4 A. H. Verbruggen, R. Griessen and J. H. Rector, *Phys. Rev. Lett., 52* (1984) 1625.
5 A. Lodder, *Solid State Commun., 71* (1989) 259.
6 R. Landauer, *Solid State Commun., 72* (1989) 867.
7 R. S. Sorbello, *Solid State Commun., 76* (1990) 747.
8 A. Lodder, *Solid State Commun., 79* (1991) 143.
9 A. Lodder, *Solid State Commun., 79* (1991) 147.
10 H. Wipf, *Top. Appl. Phys., 29* (1978) 273.
11 *Top. Appl. Phys., 29* (1978).
12 V. Erckmann and H. Wipf, *Phys. Rev. Lett., 37* (1976) 341.
13 R. A. Oriani and O. D. Gonzales, *Trans. Metall. Soc. AIME, 239* (1967) 1041.
14 J.-F. Marêché, J.-C. Rat and A. Hérold, *CR Acad. Sci., 281* (1975) 449.
15 H. L. M. Bakker, M. J. C. de Jong, P. M. Oppeneer, R. Griessen, A. Lodder, R. Vis and H. Brodowsky, *J. Phys. F, 16* (1986) 707.
16 W. Maier and H. Wipf, *Scripta Metall., 11* (1977) 695.
17 K. Watanabe and Y. Fukai, *J. Phys. F, 10* (1980) 1795.
18 A. Lodder, *J. Phys. F, 6* (1976) 1885.
19 A. Lodder, *J. Phys. F, 14* (1984) 2943.
20 R. S. Sorbello, A. Lodder and S. J. Hoving, *Phys. Rev. B, 25* (1982) 6178.
21 J. Korringa, *Physica, 13* (1947) 392.
22 W. Kohn and N. Rostoker, *Phys. Rev., 94* (1954) 1111.
23 P. M. Oppeneer and A. Lodder, *J. Phys. F, 17* (1987) 1901.
24 J. van Ek and A. Lodder, *J. Phys.: Cond. Matt., 3* (1991) 7331.
25 J. van Ek and A. Lodder, *J. Phys.: Cond. Matt., 3* (1991) 7307.
26 J. van Ek and A. Lodder, *J. Phys.: Cond. Matt., 3* (1991) 7363.
27 J. M. Ziman, *Principles of the Theory of Solids*, Cambridge University Press, Cambridge, 1972.
28 L. F. Mattheiss, *Phys. Rev., 134* (1964) 970.
29 J. P. Desclaux, C. M. Moser and G. Verhaegen, *J. Phys. B, 4* (1971) 296.
30 V. L. Moruzzi, J. F. Janak and A. R. Williams, *Calculated Electronic Properties of Metals*, Pergamon, New York, NY, 1978.
31 G. Lehmann, *Phys. Status Solidi B, 70* (1975) 737.
32 K. M. Mackay and R. A. Mackay, *Introduction to Modern Inorganic Chemistry*, 3rd edn., International Textbook Company, London, 1981.
33 P. Pyykkö, *Adv. Quantum Chem., 2* (1978) 353.
34 C. Kittel, *Introduction to Solid State Physics*, Wiley, New York, NY, 1965.
35 M. J. Puska and R. M. Nieminen, *Phys. Rev. B, 29* (1984) 5382.
36 P. M. Oppeneer and A. Lodder, *J. Phys. F, 17* (1987) 1885.
37 J. van Ek and A. Lodder, *Phys. Lett. A, 144* (1990) 379.
38 J. van Ek and A. Lodder, *Solid State Commun., 73* (1990) 373.
39 O. N. Carlson, F. A. Schmidt and D. T. Peterson, *J. Less-Common Met., 10* (1966) 1.
40 J. E. Bonnet, C. Juckum and A. Lucasson, *J. Phys. F, 12* (1982) 699.
41 *Landolt-Börnstein New Series*, Vol. 15a, Springer, Berlin, 1982.